**Power Electronic Systems
Laboratory**

Design of a Test Bench for a Lateral Stator Electrical Machine

A. Tüysüz
D. Koller
A. Looser
J. W. Kolar
C. Zwyssig

ETH
Eidgenössische Technische Hochschule Zürich
Swiss Federal Institute of Technology Zurich

Design of a Test Bench for a Lateral Stator Electrical Machine

A. Tüysüz, D. Koller, A. Looser, and J.W. Kolar
Power Electronic Systems Laboratory
ETH Zurich
CH-8092 Zurich, Switzerland
tuysuz@lem.ee.ethz.ch

C. Zwyssig
Celeroton AG
Technoparkstrasse 1
CH-8005 Zurich, Switzerland
christof.zwyssig@celeroton.com

Abstract – **In a previous study, lateral stator electrical machines have been proposed for micro-machining applications where the space in the tool head is limited. In this paper, the construction of a lateral stator machine merged into a test bench is described. The test bench is used for measuring the standstill torque of the machine in a configuration without bearings, such that only the electromagnetic torque is measured. Moreover, the test bench can be modified to measure the no-load losses and separate mechanical and electromagnetic components of it using a novel method. Further separation of different components of electromagnetic no-load losses is also discussed. Although described on a lateral stator machine, the methodology in this paper can be applied to any electrical machine.**

I. INTRODUCTION

In the last few years, several studies dealing with design, optimization and testing of high-speed electrical drives have been published [1-11]. In [12], the authors have grouped the application areas of those high-speed electrical drives into two groups: group of applications with one working point and group of applications where the drive needs to cover a wide torque-speed range. Turbo compressors are a good example of the first group whereas applications like micro-machining spindles belong to the second group. Furthermore, in [12], lateral stator electrical machines are proposed for the second group of applications in order to fit the motor in confined spaces around the rotor, while still maintaining the wide operating range. In the same paper, this wide operating range is characterized by two operating points: a low-speed high-torque operating point where all the high-speed losses such as the core losses in the stator and eddy current losses in the solid bodies are neglected; and a high-speed low-torque operating point, where the copper losses in the windings are neglected. The machine geometry is optimized using a parametric finite element method (FEM) simulation.

In this paper, further considerations about building the lateral stator machine are described in detail. Moreover, the lateral stator machine is merged into a test bench which can evaluate the machine performance in the two operating points mentioned above, enabling a direct verification of the FEM simulations. This is done by modifying the test bench into two different setups, one measuring the torque at standstill, the other measuring the no-load losses at higher speeds. The first setup is called the static torque measurement setup and the second one is named as the high-speed loss measurement setup. In the static torque measurement setup, a bearingless configuration is designed, and the torque is measured on the stator side. This allows for the measurement of the electromagnetic torque only, without the bearing friction, which enables a direct verification of the FEM analysis.

In the high-speed loss measurement setup, deceleration tests are used to measure the total no-load losses. A novel method of loss segregation is proposed which allows for the separation of the mechanical losses from the electromagnetic losses, overcoming the problem of changing bearing friction loss with changing preload. This is especially important with high-speed, low-torque electrical machines where bearing friction causes an important part of the no-load losses. Moreover, the segregation of the different components of the no-load losses is discussed.

Although the test bench design is described for a special electrical machine type, the methodology can be used to test any other electrical machine in similar way.

II. TEST BENCH DESIGN

The active parts of a lateral stator machine are the stator consisting of the lateral stator, windings and the shielding iron; and the rotor, consisting of the rotor steel and the permanent magnets. These components of the machine are responsible for the electromechanical performance of the machine such as torque and losses, and called the active components accordingly. The active parts of the lateral stator machine are shown in Fig. 1.

The first task of the test bench described in this paper is to position those active components correctly in respect to each other, in other words, to keep the active components in their places during operation. The positioning is ensured by the machine case consisting of the plastic chamber and the housing around it. The plastic chamber and surrounding
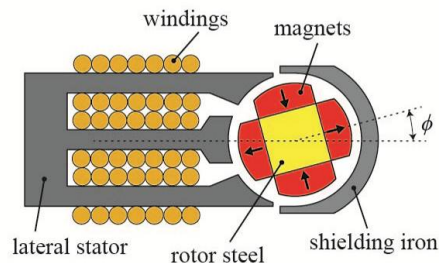

Fig. 1. Active parts of the lateral stator electrical machine. Grey parts are built of amorphous iron laminations, red parts are made of NdFeB sintered magnets (arrows indicate magnetization direction) and the yellow part is made out of cobalt-iron steel.

housing are called the passive parts and they are shown in Fig. 2, along with the active parts. The design of the passive parts is described in detail in section A.

The second task of the test bench is to measure the standstill torque of the lateral stator machine, in a bearingless configuration. This corresponds to evaluating the machine performance in the low-speed, high-torque operating point. The torque of the machine is measured on the stator side, using a reaction torque sensor. Further information on the static torque measurement setup is given in section B.

The third task of the test bench, the measurement of the no-load losses, is realized using the high-speed loss measurement setup. This corresponds to the evaluation of the lateral stator machine in the high-speed low-torque operating point, and is discussed in section C, along with options of separating different components of the no-load losses.

A. Machine Case Design

The machine case consists of two parts, a plastic chamber surrounding the lateral stator and shielding iron, and an aluminum case built around this plastic chamber. The plastic chamber needs to fulfill the following requirements:

- Nonconductive, hence no eddy current losses caused by the rotor flux or the stray flux between the stator shoes occur.
- Nonmagnetic, such that the magnetic airgap of the design can be maintained.
- Precisely machinable, in order to position the active parts correctly with respect to each other.
- Mechanically strong, to withstand the forces attracting rotor and stator parts together.

Stereolithography is chosen to build the plastic chamber in order to fulfill the design requirements listed above. ProtoTherm 12120 water-resistant resin from DSM Somos [13] has been selected as the material because of its high mechanical strength.

The plastic chamber is made of four pieces, facilitating the positioning of the lateral stator and the shielding iron. In Fig. 3a, an illustration of the plastic chamber is shown. For simplicity, only the half section views of part 3 and part 2 of the plastic chamber and only one leg of the lateral stator are depicted. It can be seen that part 3 of the plastic chamber is designed in a way that the stator legs would fit in and be aligned with respect to each other. Part 2 positions the shielding iron with respect to the lateral stator legs. Part 1 and part 4 can be taken out to take out the iron parts without changing the air gap geometry, which is formed by the circular faces of part 3 and part 2. This allows for the separation of the no-load losses (see section C). The winding ends are taken out through the empty space on part 4. The photo of the plastic chamber parts can be seen in Fig. 3b.

The housing around the plastic chamber aligns the plastic chamber (and therefore the stator) with respect to the rotor. The aluminum parts are designed in a way that it is easy to take the plastic chamber out and put it back to its position precisely, without disassembling the bearings. A photo of the machine case consisting of the plastic chamber and the aluminum housing can be seen in Fig. 4.
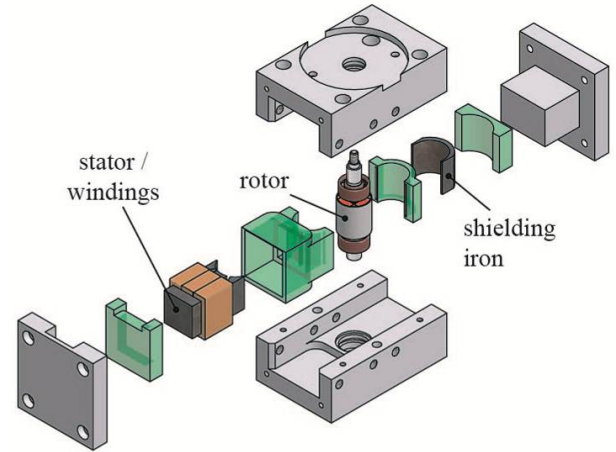

Fig. 2. Active and passive components in an exploded view of the machine case. Green parts show the plastic chamber; gray parts show the surrounding housing.

B. Static Torque Measurement Setup
1) Overview

In a permanent magnet electrical machine, torque can be described as a function of rotor position and stator currents:

$$T = f\left(\phi, i_1, i_2, i_3\right) \qquad (1)$$

where T is the torque, ϕ is the rotor's angular position and i_1, i_2, i_3 are the three-phase stator currents. The task of the static torque measurement setup is to measure this function at standstill by measuring the stator reaction torque on a bearingless configuration.

The static torque measurement setup is shown in Fig. 5 using a simplified diagram. In this setup, the rotor is fixed to the ground plate through a rotational positioning device from Standa Ltd [16]. Using this rotational positioning device, the rotor's angular position ϕ can be adjusted and fixed. The active parts of the stator (lateral stator, shielding iron and windings) which are held together by the plastic chamber and the aluminum housing are fixed to the ground plate via the piezoelectric torque transducer 9329A from Kistler. The torque transducer is connected to an oscilloscope through the
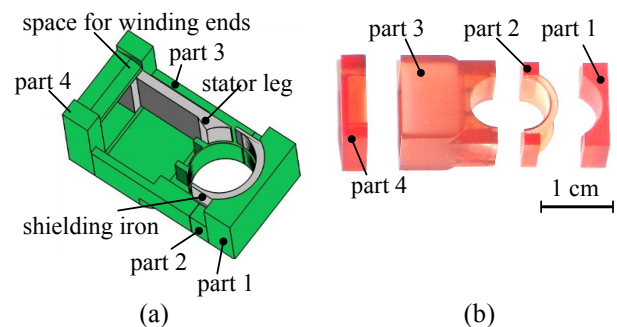

Fig. 3.   (a) Illustration of the plastic chamber parts. (b) Photo of plastic chamber parts.
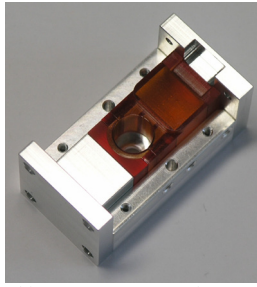
Fig. 4. Photo of the machine case (top part taken out) and the plastic chamber.

charge amplifier 5011B, also from Kistler [17]. The stator reaction torque is recorded along with instantaneous stator currents for each rotor position. Using this data, the torque function in (1) can be recreated. Fig. 6 shows a photo of the complete static torque measurement setup. The round parts of the plastic chamber facing the air gap have a thickness of 0.2 mm, resulting in a 0.6 mm magnetic air gap.

2) Finite Element Analysis of Mechanical Stresses

The lateral stator machine is not a symmetric machine by its nature. Because of this asymmetry, there is always a force pulling the rotor and the stator parts towards each other. This force depends on the rotor position and the stator currents. It has a peak value of 7.1 N for the shielding iron, 2.5 N for the rotor and 6.8 N for the lateral stator in the worst case, according to magnetic finite element analysis. Because of these forces, the lateral stator and the shielding iron push on the plastic chamber, stressing its parts facing the air gap. Furthermore, as there are no bearings on the rotor in the static torque measurement setup, the same force also bends the components holding the rotor, changing the air gap. The structural mechanics module of COMSOL Multiphysics software has been used to model these mechanical loads separately.

a. Plastic chamber

In Fig. 7, the calculated stresses and the deformation on the plastic chamber are shown. The maximum value of the von Mises stress of 2.5 MPa is far below the tensile and flexural strengths of the plastic material, which are 77 MPa and 103 MPa respectively [13], justifying the safety of the design.

b. Components holding the rotor

The stresses on the components holding the rotor is analyzed in the same way. In Fig. 8, the calculated displacement of the rotor is shown for a force of 5 N acting on the rotor, which is double the force expected in the worst case. The maximum displacement of 2.5 µm can be neglected considering the 600 µm magnetic air gap.

3) Verification of Finite Element Analysis

If the finite element model can be verified on a simple geometry, its application on a more complicated geometry can be justified. For this reason, first a new finite element model was build where only the part 1 of the plastic chamber is modeled, loaded with a 5 N point load on a stiff steel block (Fig. 9). This simple setup is then realized, and a spring scale is used to create the point load of 5 N, while the displacement is measured using a laser displacement sensor from Keyence [14].

Measured displacement is around 20 µm for different readings on the sensor. The measured value is in good accordance with the finite element analysis results for this simplified geometry, taking into account the uncertainties on the point of force application, the point of measurement, the precision of the spring scale and the sliding of the plastic part on the steel during the application of force. This verifies the mechanical FE analysis on the plastic chamber.
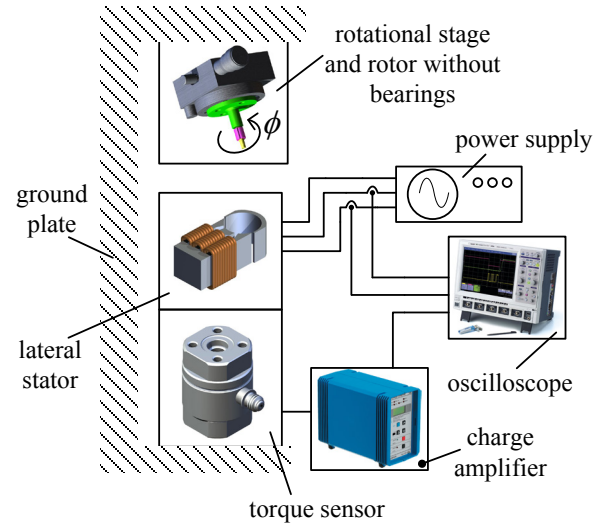

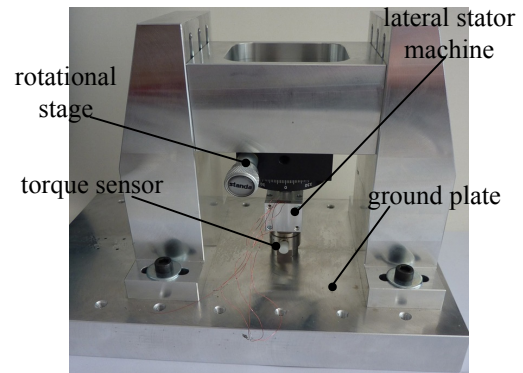Fig. 5. Block diagram of the static torque measurement setup.

Fig. 6. Photo of the complete torque measurement setup.
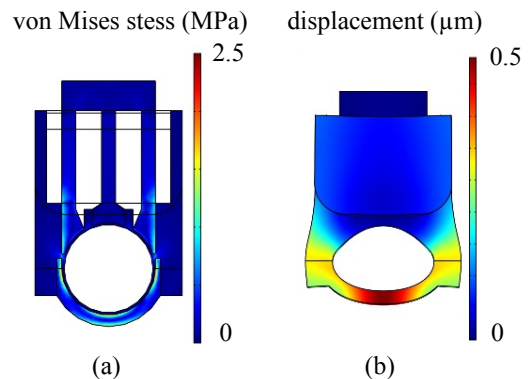

(a)   (b)

Fig. 7. Finite element analysis of the stresses on the plastic chamber.
(a)   Slice view von Mises stress on the stator and the plastic chamber.
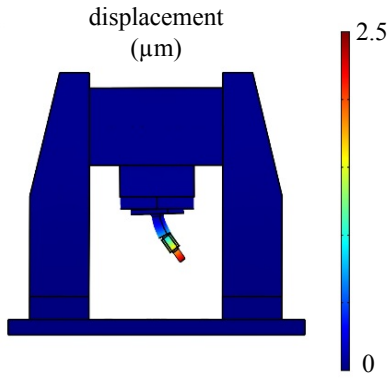(b)   Boundary view of the deformation of the plastic chamber under load.

Fig. 8. Finite element analysis of the bending of the components holding the rotor under magnetic forces.

C. High Speed Loss Measurement Setup

1) Overview

The high-speed losses considered in this paper are the mechanical friction losses (windage losses and bearing friction losses) and electromagnetic losses (rotor eddy current losses, stator core losses and proximity losses in the windings). Using the high speed loss measurement setup described in this section, those losses can be measured and segregated.

In [5], the torque of an electrical machine is calculated according to (2) by accelerating the machine and recording the angular position.

$$T_{\mathrm{m}} = J \frac{d\omega}{dt} \qquad (2)$$

where T_{m} is the total torque applied on the shaft, J is the inertia of the rotor, ω is the angular speed of the rotor and t is the time.

In similar way, if the machine is first accelerated to a certain speed and then the drive power is cut off, the braking torque caused by no-load losses can be calculated using the inertia and the deceleration of the machine. Using this deceleration test, the total no-load losses in a machine can be measured as a function of speed. However, different components of the total no-load losses cannot be separated.

In [15], a dummy rotor is proposed which is identical to the rotor of the machine, but the magnets on it are not magnetized. Using this dummy rotor, electromagnetic losses and the mechanical friction losses are separated. However,
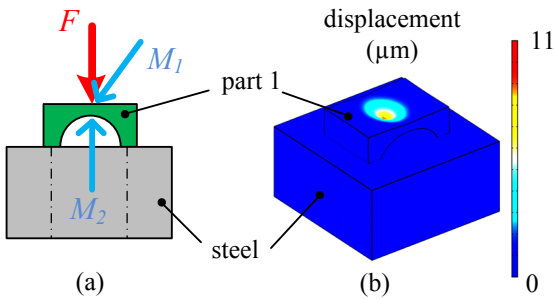

Fig. 9. (a) Direction of applied force (red) and laser displacement measurement angles (blue)
(b)Finite element analysis of a point load on the part 1 of the plastic chamber.
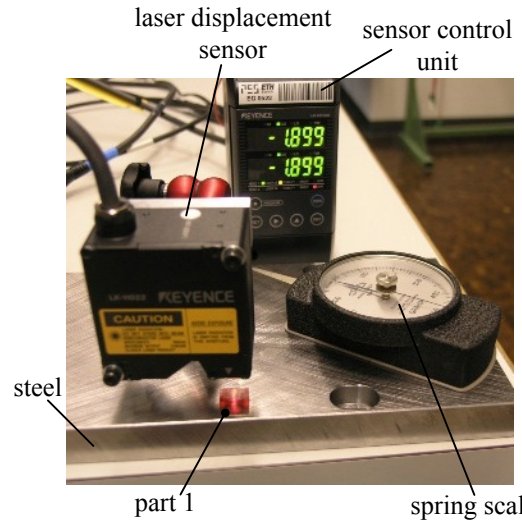

Fig. 10. Photo of the simple test setup for the verification of finite element analysis.

the bearing friction losses depend strictly on the preload, whose variation cannot be avoided or controlled easily while assembling the test bench or coupling the machine under test to a drive machine. This brings an uncertainty on the contribution of the bearing losses to the total no-load losses. At high speeds, this uncertainty can no longer be neglected.

In order to separate the electromagnetic losses from the total no-load losses, a new method is proposed. This method consists of running deceleration tests with and without the stator.

In Fig. 11, the high-speed loss measurement setup is explained with a block diagram. A commercial ultra-high-speed electrical machine from Celeroton, CM-2-500 [18], is used as a drive machine and is coupled to the lateral stator machine using an M2 thread as shown in Fig. 11. The drive machine is used to accelerate the lateral stator machine to a desired speed. Then, the drive power is cut off, and the back emf of the drive machine is recorded with an oscilloscope during deceleration. The speed is calculated using the back emf. With the speed and inertia known, the total no-load losses of the drive machine and the lateral stator machine can be calculated. After running a deceleration test on this setup, the housing of the test bench is opened on both sides to take the stator and the shielding iron out. As the bearings are not disassembled, the preload and therefore the friction losses of the bearings do not change. The plastic chamber ensures that the air gap geometry stays the same; therefore the windage losses are also the same in the setups with and without the stator. The aluminum housing of the machine case is replaced by a plastic housing of the same geometry in order to avoid any additional eddy current losses when the stator and the shielding iron are taken out. A deceleration test on this setup gives the total no-load losses of the drive machine plus only the mechanical losses of the lateral stator machine. Accordingly, the electromagnetic losses of the lateral stator machine can be extracted. Furthermore, the proximity losses can be measured in similar way, running deceleration tests with and without the windings

around the stator. In Fig. 12, a photo of the high-speed loss measurement setup is shown.

2) Finite Element Analysis of Rotordynamics

In electrical machines, the critical speeds of the rotor can be a limiting factor on the maximum achievable speed. Therefore, COMSOL Multiphysics has been used to analyze the rotor dynamics of the test bench. The bending modes of the high-speed loss measurement setup are shown in Fig. 13. It can be seen that the third bending mode which limits the speed is out of the nominal speed range of the test bench (200 000 rpm), however the first two modes occur below the rated speed. Plastic o-rings are used with the high-speed ball bearings to limit the effect of the vibrations excited at those critical speeds. The o-rings also make the construction less sensitive to misalignments during coupling the drive machine to the machine under test.
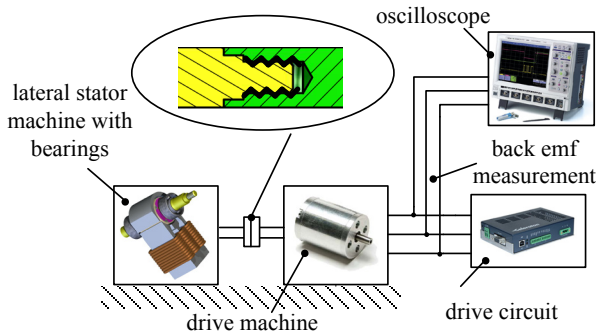

Fig. 11. Block diagram of the high speed loss measurement setup and the mechanical coupling. (yellow) lateral stator machine shaft, (green) drive machine shaft.
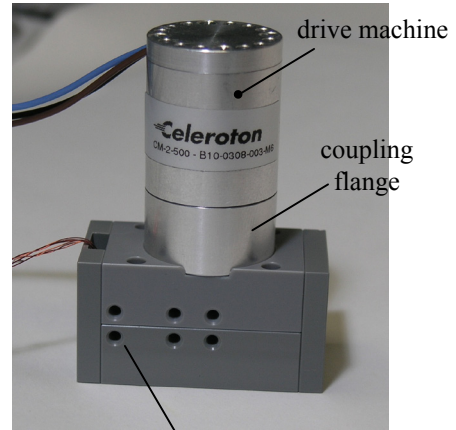
3) Further separation of electromagnetic losses

So far it has been described how the electromagnetic losses of the lateral stator machine can be separated from the total no-load losses. It has also been mentioned that the no-load proximity losses in the windings caused by the stray flux between the stator legs can be measured. In this section the separation of the eddy current losses in the rotor's solid bodies and the stator core losses is discussed.

Time-temperature tests have been being used since the early days of electrical engineering to measure the losses of electrical equipment. In [19], an electrical machine is operated under load until it reaches a constant temperature. Then, the load is turned off and the initial slope of the temperature is measured, to calculate the losses of the machine under that particular load. This method has to be modified in order to measure the no-load losses. In [20], a modified thermometric approach is presented where the losses are measured by time-temperature tests on thermally insulated stator parts.

Because all other losses can be segregated with the methods described in section C.1, in the case of a lateral stator machine, only the segregation of the stator core losses from the eddy current losses in the solid bodies of the rotor at no-load is needed to verify the losses calculated by FEM.

Time-temperature tests can be done by placing temperature sensors on the lateral stator, and measuring the temperature rise. As the precise numerical determination of the heat

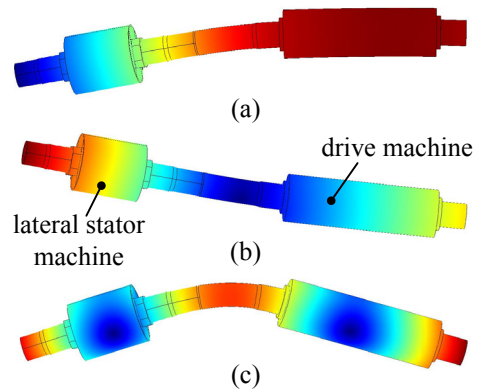Fig. 12. Photo of the high speed loss measurement setup.

Fig. 13. Bending modes of the high-speed loss measurement setup. (a) First bending mode at 2.35 kHz, 141 000 rpm; (b) second bending mode at 2.7 kHz, 162 000 rpm; (c) third bending mode at 5.4 kHz, 324 000 rpm. Blue shows no displacement, red shows maximum displacement.

transfer coefficients of the stator surface is a difficult task, only the initial slope of the temperature rise can be used with the well-defined heat capacity of the stator iron in order to estimate the losses. Therefore, the temperature has to be measured while the no-load losses are instantly turned on, in other words, when the machine is being rapidly speeded up from standstill to the no-load speed. However, in practice, the acceleration of the machine takes time, and when testing small machines with small thermal capacitances, this method may give inaccurate results if the mechanical time constant for acceleration is not negligible compared to the thermal time constant. A possible approach to overcome this problem is to thermally insulate the stator. The surrounding of the machine can be vacuumed to thermally insulate the small and complicated stator geometry. Another possible problem with the time-temperature test is the fact that the temperature sensors can only be placed on the surface of the stator, where stray field effects may result in changes in the thermal behavior compared to the rest of the stator body.

A further possible method of separating the rotor eddy current losses from the stator core losses relies on the dependency of those losses on the speed of the machine.

According to the datasheet of the stator iron material [21], the core losses are given by the Stenimetz equation:

$$P_{\text{core}} = C_m \cdot f^{1.51} \cdot \hat{B}^{\beta} \tag{3}$$

where P_{core} is the core loss density, C_m and β are constants, f is the frequency and the $\hat{B}$ is the peak value of the magnetic field density. According to [22], the eddy current losses in the permanent magnets of an electrical machine can be expressed as:

$$P_{\text{eddy}} = C_e \cdot \frac{\partial^2 B}{\partial t^2} \tag{4}$$

where P_{eddy} is the eddy current loss density, C_e is a constant, B is the magnetic field density and t is the time. This means, for a given peak value of B, the eddy current losses are proportional to the square of the frequency of excitation. Therefore, if the total no-load losses are known as a function of rotor speed, the core losses which are proportional to $f^{1.51}$ and the eddy current losses which are proportional to f^2 can be separated using a curve fitting approach. It should be noted that this approach neglects the effect of the eddy currents on the magnetic field, considering a constant B over the speed (frequency) range at no-load. This assumption has been justified for the lateral stator machine by using Maxwell software package from Ansoft. Two 3D models of the lateral stator machine were analyzed at no-load, one neglecting and the other accounting for the eddy current and core loss effect on the field solution according to [23]. The difference of iron losses obtained in both cases were within 10% at the maximum speed, showing that the effect of the eddy currents on the field solution is negligible, allowing the curve fitting approach to be used for separation of eddy currents from the stator core losses.

III. CONCLUSION

The construction of a lateral stator machine in a test bench is described. Using this test bench, the static torque of the machine can be measured without the bearing friction; therefore the finite element analysis carried out during the design of the machine can be verified. In a modified test setup, the total no-load losses of the machine can be measured, and the electromagnetic losses can be separated from the mechanical friction losses using a novel method. Additionally, two different methods for separation of the components of the no-load electromagnetic losses are discussed.

The measurements taken on the test bench are going to be published in the next publications. Future work also includes experimental comparison of electromagnetic loss segregation methods described.

REFERENCES

[1] D. Krähenbühl, C. Zwyssig, H. Weser, and J.W. Kolar, "A miniature, 500 000 rpm, electrically driven turbocompressor," *Energy Conversion Congress and Exposition, ECCE*, pp.3602-3608, Sept. 2009.

[2] D. Krähenbühl, C. Zwyssig, K. Bitterli, M. Imhof, and J.W. Kolar, "Evaluation of ultra-compact rectifiers for low power, high-speed, permanent-magnet generators," *35th Annual Conference of Ind. Electronics, IECON*, pp. 448-455, Nov. 2009.

[3] M. Morimoto, K. Aiba, T. Sakurai, A. Hoshino, and M. Fujiwara, "Position sensorless starting of super high-speed PM generator for micro gas turbine," *IEEE Trans. on Ind. Electron.*, vol. 53, no. 2, pp. 415–420, Apr. 2006.

[4] I. Takahashi, T. Koganezawa, G. Su, and K. Ohyama, "A super high speed PM motor drive system by a quasi-current source inverter", *IEEE Trans. Ind. Appl.*, vol. 30, no. 3, pp. 683-690, May/June 1994.

[5] P. D. Pfister and Y. Perriard, "Very-high-speed slotless permanent-magnet motors: analytical modeling, optimization, design, and torque measurement methods," *IEEE Trans. on Ind. Electron.*, vol. 57, no. 1, pp. 296-303, Jan. 2010.

[6] L. Zhao, C. Ham, L. Zheng, T. Wu, K. Sundaram, J. Kapat, and L. Chow, "A highly efficient 200 000 rpm permanent-magnet motor system," *IEEE Trans. on Magn.*, vol. 43, no. 6, pp. 2528–2530, June 2007.

[7] C. Zwyssig, S. D. Round, and J. W. Kolar, "An ultrahigh-speed, low power electrical drive system," *IEEE Trans. on Ind. Electron.*, vol. 55, no. 2, pp. 577 - 585, Feb. 2008.

[8] M. A. Rahman, A. Chiba, and T. Fukao, "Super high speed electrical machines – summary," in *Proc. of IEEE Power Engineering Society General Meeting*, vol. 2, pp. 1272-1275, June 2004.

[9] A. Binder and T. Schneider, "High-speed inverter-fed AC drives," *International Aegean Conference on Electrical Machines and Power Electronics, Electromotion*, Sept. 2007.

[10] A. Borisavljevic, H. Polinder, and J. A. Ferreira, "On the speed limits of permanent-magnet machines," *IEEE Trans. on Ind. Electron.*, vol. 57, no. 1, pp. 220-227, Jan. 2010.

[11] M. H. Kimman, H. H. Langen, J. van Eijk, and R. M. Schmidt, "Design and realization of a miniature spindle test setup with active magnetic bearings," *IEEE/ASME International Conference on Advanced Intelligent Mechatronics*, pp.1-6, Sept. 2007.

[12] A. Tüysüz, A. Looser, C. Zwyssig, and J.W. Kolar, "Novel miniature motors with lateral stator for a wide torque and speed range," *36th Annual Conference of Ind. Electronics, IECON*, pp. 1741-1747, Nov. 2010.

[13] DSM Somos, Internet: www.dsm.com, online on March 2011.

[14] Keyence Corp. Internet: www.keyence.com, online on March 2011.

[15] A. S. Nagorny, "A simple and accurate method for the experimental performance evaluation of high speed sensorless brushless dc motors," *Electric Machines and Drives Conference, IEMDC*, pp. 916-921, May 2009.

[16] Standa Ltd., "7R7 Mini Rotational Stage," Internet: http://www.standa.lt/products/catalog/ , online on March 2011.

[17] Kistler Instrumente AG, Internet: www.kistler.com, online on March 2011.

[18] Celeroton AG, www.celeroton.com, online on March 2011.

[19] M.D. Ross, "Time-temperature tests to determine Machine Losses," *Trans. of the AIEE*, vol. 54, no.2, pp 515-515, May 1935.

[20] N. Dehlinger and M.R. Dubois, "A simple insulated thermometric method for the experimental determination of iron losses," *18th Int. Conf. on Electrical Machines*, pp. 1-6, Sept. 2008.

[21] Metglas Inc., "Powerlite forms, 2605SA1," *Technical Bulletins*, Internet: www. metglas.com/tech/index.htm, online on March 2011.

[22] S. Ruoho, T. Santa-Nokki, J. Kolehmainen and A. Arkkio, "Modeling magnet length in 2-D finite-element analysis of electric machines," *IEEE Trans. on Magn.*, vol. 45, no. 8, pp. 3114–3120, Aug. 2009.

[23] D. Lin, P_ Zhou, Q.M. Chen, N. Lambert amd Z.J. Cendes, "The effects of steel lamination core losses on 3D transient magnetic fields," *IEEE Trans. on Magn.*, vol. 46, no. 8, pp. 3539–3542, Aug. 2010.